Substorm dependence of plasmaspheric hiss

Nigel P. Meredith,[1] Richard B. Horne,[2] Richard M. Thorne,[3] Danny Summers,[4,5] and Roger R. Anderson[6]

Received 13 January 2004; revised 5 April 2004; accepted 15 April 2004; published 15 June 2004.

[1] We analyze wave and particle data from the CRRES satellite to determine the variability of plasmaspheric hiss ($0.1 < f < 2$ kHz) with respect to substorm activity as measured by *AE**, defined as the maximum value of the *AE* index in the previous 3 hours. The study is relevant to modeling the acceleration and loss of relativistic electrons during storms and understanding the origin of the waves. The plasmaspheric hiss amplitudes depend on spatial location and susbtorm activity, with the largest waves being observed during high levels of substorm activity. Our survey of the global distribution of hiss indicates a strong day-night asymmetry with two distinct latitudinal zones of peak wave activity primarily on the dayside. Equatorial hiss ($|\lambda_m| < 15°$) is strongest during active conditions (*AE** > 500 nT), with an average amplitude of 40 ± 1 pT observed in the region $2 < L < 4$ from 0600 to 2100 MLT. Midlatitude ($|\lambda_m| > 15°$) hiss is strongest during active conditions with an average amplitude of 47 ± 2 pT in the region $2 < L < 4$ from 0800 to 1800 MLT but extending out beyond $L = 6$ from 1200 to 1500 MLT. Equatorial hiss at 600 Hz has minimum cyclotron resonant energies ranging from ~20 keV at $L = 6$ to ~1 MeV at $L = 2$, whereas midlatitude hiss at 600 Hz has minimum resonant energies ranging from ~50 keV at $L = 6$ to ~2 MeV at $L = 2$. The enhanced equatorial and midlatitude hiss emissions are associated with electron flux enhancements in the energy range of tens to hundreds of keV, suggesting that these electrons are the most likely source of plasmaspheric hiss. The enhanced levels of plasmaspheric hiss during substorm activity will lead to increased pitch-angle scattering of energetic electrons and may play an important role in relativistic electron dynamics during storms. *INDEX TERMS:* 2730 Magnetospheric Physics: Magnetosphere—inner; 2768 Magnetospheric Physics: Plasmasphere; 2772 Magnetospheric Physics: Plasma waves and instabilities; 7867 Space Plasma Physics: Wave/particle interactions; 2716 Magnetospheric Physics: Energetic particles, precipitating; *KEYWORDS:* inner magnetosphere, wave-particle interactions, plasmaspheric hiss, substorms, energetic electrons, relativistic electrons

Citation: Meredith, N. P., R. B. Horne, R. M. Thorne, D. Summers, and R. R. Anderson (2004), Substorm dependence of plasmaspheric hiss, *J. Geophys. Res.*, *109*, A06209, doi:10.1029/2004JA010387.

1. Introduction

[2] Plasmaspheric hiss is a broadband, structureless, extremely low frequency (ELF) electromagnetic emission, which occurs in the frequency range from ~100 Hz to several kHz. This natural whistler mode emission is characteristically confined to higher-density regions associated with the Earth's plasmasphere [*Dunckel and Helliwell*, 1969; *Russell et al.*, 1969; *Thorne et al.*, 1973] or detached plasma regions [*Chan and Holzer*, 1976; *Cornilleau-Wehrlin et al.*, 1978; *Parrot and Lefeuvre*, 1986]. Plasmaspheric hiss can persist during relatively quiet conditions, but the emission intensifies during magnetic storms or substorms [*Smith et al.*, 1974; *Thorne et al.*, 1974, 1977]. Wave intensification has been associated with the injection of plasma sheet electrons into the inner magnetosphere during substorms [*Thorne and Barfield*, 1976; *Solomon et al.*, 1988; *Cornilleau-Wehrlin et al.*, 1993].

[3] Broadband amplitudes of plasmaspheric hiss typically range between 10 pT or less during geomagnetically quiet conditions [*Thorne et al.*, 1973], to as high as 100 pT during the recovery phase of storms [*Smith et al.*, 1974]. Plasmaspheric hiss appears to propagate over a broad range of wave-normal angles, with predominantly field-aligned propagation near the geomagnetic equator

[1]Mullard Space Science Laboratory, University College London, Holmbury St. Mary, Surrey, UK.
[2]British Antarctic Survey, Natural Environment Research Council, Cambridge, UK.
[3]Department of Atmospheric Sciences, University of California, Los Angeles, California, USA.
[4]Department of Mathematics and Statistics, Memorial University of Newfoundland, St. John's, Newfoundland, Canada.
[5]Also at School of Physics, University of KwaZulu-Natal, Durban, South Africa.
[6]Department of Physics and Astronomy, The University of Iowa, Iowa City, Iowa, USA.

0148-0227/04/2004JA010387$09.00

[*Parrot and Lefeuvre*, 1986; *Santolik et al.*, 2001] and more oblique propagation at higher latitudes.

[4] Despite extensive observations, the generation mechanism of plasmaspheric hiss has not been fully resolved. Early theoretical studies [*Kennel and Petschek*, 1966; *Kennel and Thorne*, 1967; *Thorne et al.*, 1973, 1979] established the importance of electron cyclotron resonance instability occurring near the magnetic equatorial plane. Maximum rates of wave amplification occur when whistler mode waves propagate parallel to the ambient magnetic field near the equator. Oblique waves are usually found away from the equator and generally suffer net damping [*Kennel and Thorne*, 1967]. Because the rate of convective wave growth is relatively low inside the plasmapause, *Thorne et al.* [1979] suggested that the cyclotron resonance mechanism can best be maintained by amplified waves that return repeatedly to the equatorial region after magnetospheric reflection [*Thorne and Kennel*, 1967], as long as the waves return to the equator approximately field-aligned. Using ray tracing techniques, *Huang et al.* [1983], *Church and Thorne* [1983], and *Storey et al.* [1991] tested the viability of the generation of plasmaspheric hiss by the electron cyclotron resonance mechanism. *Huang et al.* [1983] and *Storey et al.* [1991] found that waves launched at small wave-normal angles at the equator received insignificant amplification after the first magnetospheric reflection. In contrast, the study of *Church and Thorne* [1983] confirmed the importance of the recycling process for the excitation of plasmaspheric hiss. A possible reason for the contrasting conclusions in these studies is the adoption of differing models of the magnetospheric electron number density distribution. All three studies confirmed that waves launched near the magnetic equator propagate with increasing wave normal angles at higher latitude and consequently suffer Landau damping, primarily from electrons with energies of $\sim$1 keV. Detailed analyses of the cyclotron resonance generation mechanism inside the plasmapause [*Solomon et al.*, 1988; *Cornilleau-Wehrlin et al.*, 1993] showed that hiss amplification can be achieved on a single wave transit (within 10°) of the magnetic equator.

[5] Plasmaspheric hiss is an important constituent of the Earth's magnetospheric plasma environment. Resonant pitch-angle scattering of energetic electrons by plasmaspheric hiss largely accounts for the formation of the slot region that separates the inner ($1.3 < L < 2.5$) and outer ($3 < L < 7$) radiation belts and contributes to the overall structure of the electron radiation belt [*Lyons et al.*, 1972; *Lyons and Thorne*, 1973; *Albert*, 1994; *Abel and Thorne*, 1998a, 1998b]. Relativistic (>1 MeV) electrons, which are often generated in the inner magnetosphere during magnetic storms, are subject to gradual decay as a result of pitch-angle scattering by plasmaspheric hiss over the extended recovery phase of a storm [*Spjeldvik and Thorne*, 1975]. Accurate quantification of electron losses due to resonant pitch-angle scattering by plasmaspheric hiss (and other plasma waves) is therefore essential for the development of models of the variability of storm-time relativistic electrons. This paper provides a synoptic analysis of the global distribution of plasmaspheric hiss and its variability during substorm activity. Our results can be used to further the understanding of the origin of the waves and as a basis for evaluating the rates of energetic electron scattering during storm conditions.

2. Instrumentation and Data Analysis

[6] The Combined Release and Radiation Effects Satellite (CRRES) is particularly well-suited to studies of wave-particle interactions in the radiation belts both because of its orbit and sophisticated suite of wave and particle instruments. The spacecraft was launched on 25 July 1990 and operated in a highly elliptical geosynchronous transfer orbit with a perigee of 305 km, an apogee of 35,768 km, and an inclination of 18°. The orbital period was approximately 10 hours, and the initial apogee was at a magnetic local time of 0800 MLT. The satellite swept through the heart of the radiation belts on average approximately 5 times per day, providing good coverage of this important region for almost 15 months.

[7] The wave data used in this study were provided by the Plasma Wave Experiment on board the CRRES spacecraft. This experiment provided measurements of electric fields from 5.6 Hz to 400 kHz, using a 100 m tip-to-tip long wire antenna, with a dynamic range covering a factor of at least 10^5 in amplitude [*Anderson et al.*, 1992]. The electric field detector was thus able to detect waves from below the lower hybrid resonance frequency (f_{LHR}) to well above the upper hybrid resonance frequency (f_{UHR}) for a large fraction of each orbit.

[8] Low-energy electron data used in this study were collected by the Low-Energy Plasma Analyser (LEPA). This instrument consisted of two electrostatic analyzers with microchannel plate detectors, each with a field of view of 120° × 5°, one measuring electrons and the other ions in the energy range 100 eV < E < 30 keV [*Hardy et al.*, 1993]. The instrument detected the complete pitch angle range from 0° to 180° every 30 s with a resolution of 5.625° × 8° at 20 energy channels in the range 100 eV < E < 30 keV.

[9] Higher-energy electron data were collected by the Medium Electrons A (MEA) experiment. This instrument, which used momentum analysis in a solenoidal field, had 17 energy channels ranging from 153 keV to 1.58 MeV [*Vampola et al.*, 1992]. The full field of view, coupled with the angular scan of 6° which occurred during the 0.512 s data accumulation period, resulted in a total acceptance angle of 8°–18°, depending on the channel.

2.1. CRRES Database

[10] In order to perform a statistical analysis of the wave amplitudes of plasmaspheric hiss and their relationship to the electron flux, we constructed a database from the wave and particle data. The wave data were initially corrected for the instrumental background response and smoothed by using a running 3-min average to take out the beating effects due to differences in the sampling and the spin rate. Spurious data points, data spikes, and periods of instrumental downtime were flagged and ignored in the subsequent statistical analyses. Twelve orbits, during which nontraditional configurations were deployed for testing purposes, were also excluded from the analyses.

[11] Since energy and pitch-angle diffusion rates scale as the square of the magnetic field amplitude [*Kennel and Engelmann*, 1966], the observed electric field spectral

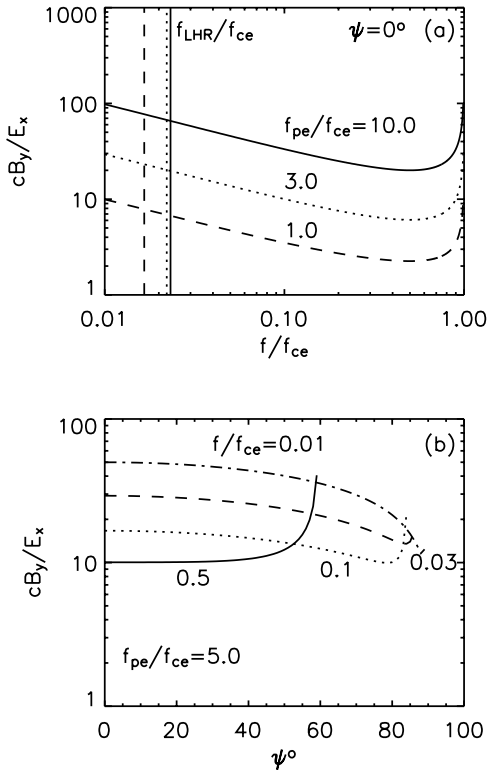

Figure 1. The derived magnetic field amplitude as a function of (a) normalized frequency and (b) wave normal angle for different ratios of f_{pe}/f_{ce}, assuming an electric field wave amplitude of 1 mVm^{-1}.

intensities, S_E, below the electron gyrofrequency f_{ce}, were first converted to magnetic field spectral intensities, S_B, using the expression

$$S_B = \frac{1}{c^2}\left(1 - \frac{f_{pe}^2}{f(f - f_{ce})}\right) S_E \qquad (1)$$

derived from Maxwell's third equation, and assuming a cold plasma dispersion relation for parallel-propagating ($\psi = 0°$) whistler mode waves. Here c is the speed of light, f is the wave frequency, f_{ce} is the electron gyrofrequency, and f_{pe} is the electron plasma frequency. The electron plasma frequency was estimated from the observations of electrostatic waves at the upper hybrid frequency and the low-frequency cut-off of electromagnetic continuum radiation, as described by *Meredith et al.* [2002b]. The electron gyrofrequency f_{ce} was determined from the fluxgate magnetometer instrument on board the spacecraft [*Singer et al.*, 1992]. The calculation of S_B can be successfully applied in the region $L > \sim 2$. At lower L, f_{pe} is too high to be obtained from the wave instrument.

[12] Magnetic field wave intensities over the frequency range $0.1 < f < 2$ kHz were then defined by an integral of the averaged wave spectral intensity (pT^2 Hz^{-1}). The corresponding wave amplitudes were then obtained by taking the square root of the wave intensities. Figure 1 (upper panel) indicates that the conversion to magnetic field amplitudes is strongly dependent on normalized wave frequency and the ratio f_{pe}/f_{ce}. For a wave frequency of 600 Hz, inside a typical band of plasmaspheric hiss, just inside the plasmapause (where $f_{pe}/f_{ce} \sim 10$) a measured electric field of 1 mV m^{-1} yields a magnetic wave amplitude of ~130 pT. The lower panel of Figure 1 indicates that for $f/f_{ce} < 0.5$ the conversion from electric to magnetic fields is relatively insensitive to wave normal angle for $\psi < 50°$, thereby justifying the use of the approximation in equation (1).

[13] To help better identify high-density regions and to distinguish between plasmaspheric hiss and other types of emissions such as whistler mode chorus (discussed below), data on electrostatic electron cyclotron harmonic (ECH) wave amplitudes were also analysed. The wave amplitudes were determined by integrating the averaged wave electric field spectral intensity ($V^2m^{-2}Hz^{-1}$) over the frequency range $f_{ce} < f < 2f_{ce}$ and taking the square root of the integrated spectral intensity. Thermal noise also contributes to the wave amplitude in this frequency band, but for the sake of simplicity, the waves observed in this band will henceforth be referred to as ECH waves.

[14] Magnetic field amplitudes in the range $0.1 < f < 2$ kHz, electric field amplitudes between $f_{ce} < f < 2f_{ce}$, and electron perpendicular differential number flux for each energy level of the LEPA and MEA instruments were then rebinned as a function of half orbit (outbound and inbound) and L in steps of $0.1L$. The data were recorded together with the universal time (UT), magnetic latitude (λ_m), magnetic local time (MLT), substorm and geomagnetic activity indices *AE* and *Kp*, and time spent in each bin with the same resolution.

3. CRRES Wave Observations

[15] An example of enhanced plasmaspheric hiss, which occurred during a period of substorm activity as monitored by the AE index, is shown in Figure 2. The wave electric field spectral intensity is plotted against UT for the entire orbit beginning at perigee at 1742:18 UT on 12 September 1990 and ending at the next perigee at 0248:50 UT on 13 September 1990. The magnetic local time, magnetic latitude and L-value are also given at hourly intervals. The solid white line shows the value of f_{ce}, determined from the measured ambient magnetic field, and the dashed white lines below f_{ce} represent $0.5f_{ce}$, $0.1f_{ce}$, and the lower hybrid resonance frequency, f_{LHR}. The dotted white lines above f_{ce} correspond to the first four harmonics of f_{ce}. The solid red line denotes the upper hybrid resonance frequency $f_{UHR} = (f_{pe}^2 + f_{ce}^2)^{1/2}$ calculated from the lower-frequency cut-off of the electromagnetic continuum, and the red dashed line is f_{UHR} calculated from wave emissions at f_{UHR} inside the plasmapause.

[16] Starting from perigee at 1742:18 UT and continuing to the outbound plasmapause crossing at ~1836 UT, weak nightside plasmaspheric hiss is observed below 2 kHz. This emission appears to be unrelated to any of the characteristic frequencies of the plasma. Enhanced upper-band ($0.5f_{ce} < f < f_{ce}$) and lower-band ($0.1f_{ce} < f < 0.5f_{ce}$) chorus emissions are seen as the spacecraft exits the plasmapause. These emissions show a drop in intensity at approximately $0.5f_{ce}$ and are an example of double-banded chorus reported by previous workers [*Tsurutani*

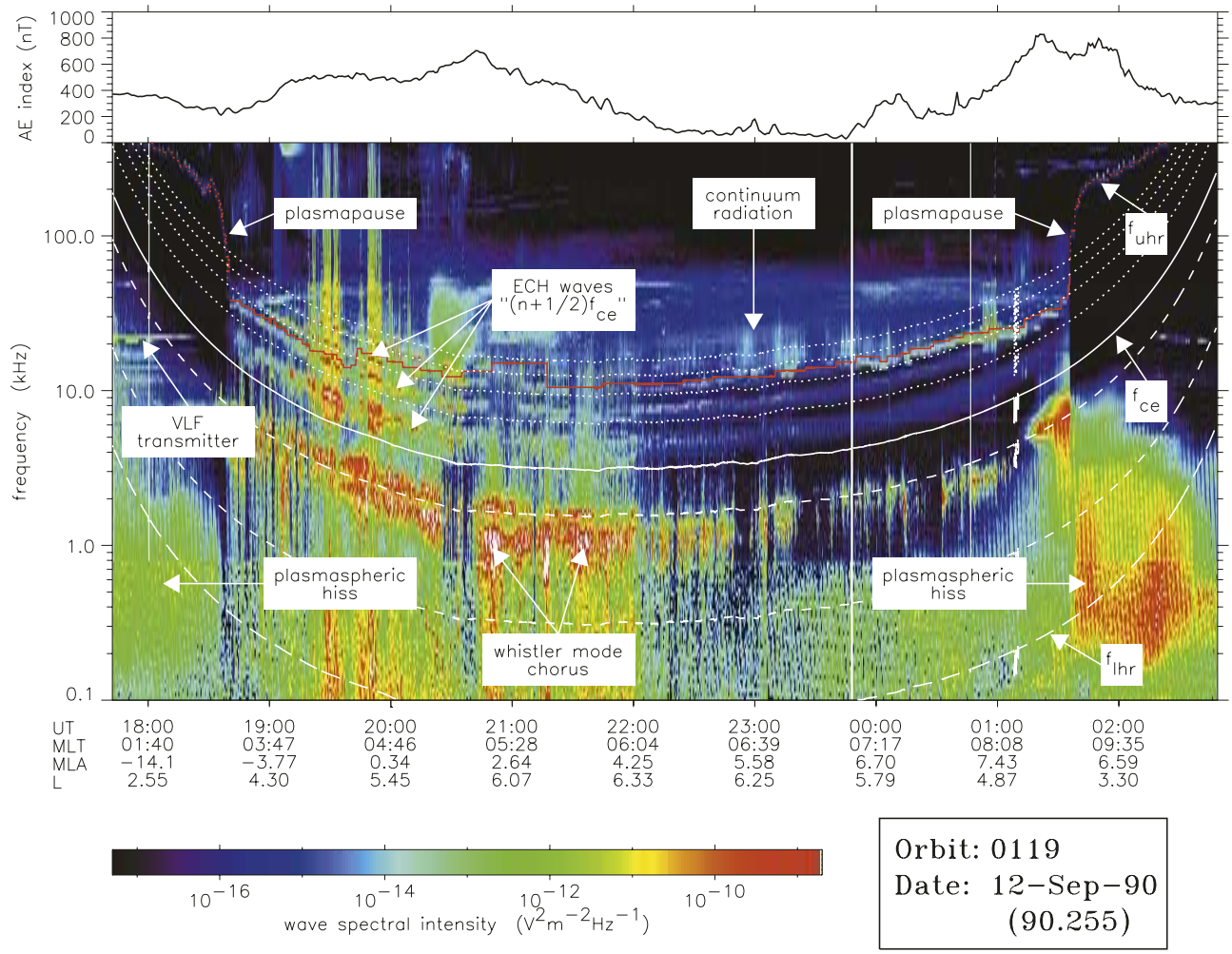

Figure 2. Survey plot of the wave spectral intensity observed on CRRES during orbit 119 together with a trace of the AE index (top). Plasmaspheric hiss is the unstructured emission below a few kHz, which is primarily confined to the plasmasphere. The solid white line represents the local electron gyrofrequency f_{ce}. Dashed lines from bottom to top represent the local lower hybrid resonance frequency f_{LHR}, $0.1f_{ce}$, and $0.5f_{ce}$. The first four harmonics of f_{ce} are represented by the dotted lines and the local upper hybrid resonance frequency f_{UHR} is shown in red.

and Smith, 1974]. Chorus emissions remain enhanced until about 2200 UT, when the *AE* index falls below 200 nT. Much weaker bursts of chorus are subsequently observed intermittently until the spacecraft reenters the plasmasphere at ~0138 UT. Enhanced electron cyclotron harmonic (ECH) waves are observed from the outbound crossing of the plasmapause at 1836 UT until 2200 UT. These waves, which propagate between the harmonics of the electron gyrofrequency, are substorm-dependent and tend to maximize in the equatorial region [e.g., *Gough et al.*, 1979; *Belmont et al.*, 1983; *Meredith et al.*, 2000]. However, a combination of weaker ECH emissions and thermal noise (which is damped at harmonics of the gyrofrequency) are observed on the inbound pass right up until the spacecraft reenters the plamasphere at 0138 UT. The chorus and ECH wave activity then abruptly cease and are replaced by strong plasmaspheric hiss emissions below about 3 kHz. The horizontal lines between 10 and 25 kHz before 1830 UT and after 0200 UT are from ground-based VLF transmitters used for navigation and communication with submarines.

3.1. Identification of Plasmaspheric Hiss

[17] The wave spectrogram in Figure 2 shows that lower-band chorus can fall into the nominal frequency range of plasmaspheric hiss ($0.1 < f < 2$ kHz) outside $L \sim 3.5$. Distinguishing between hiss and chorus is problematic on time-averaged data, particularly at large L. Hiss emissions tend to be confined to the region inside of the plasmapause where the plasma density is high, whereas whistler mode chorus activity is usually observed outside the plasmapause. However, hiss can propagate out of the plasmapause, making identification difficult. At first we tried setting a limit such that hiss would be identified only in regions where f_{pe} was sufficiently large, but, by inspection, this omitted a significant number of events during relatively quiet conditions where the plasmapause has no distinct "edge" and the plasma density falls gradually with L. Our

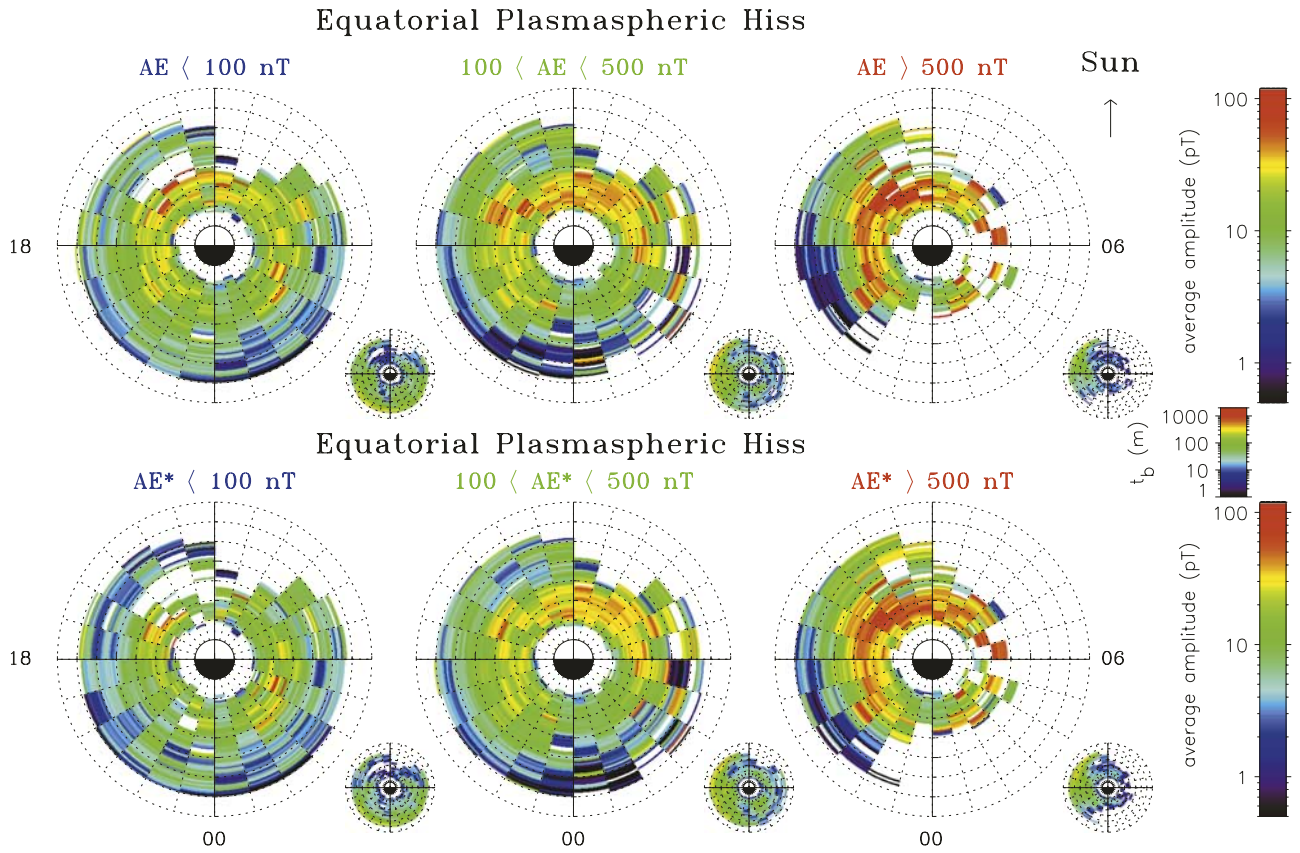

Figure 3. The average equatorial hiss magnetic field wave amplitude as a function of L and MLT for different levels of substorm activity based on the instantaneous value of the *AE* index (upper panels) and *AE** (lower panels). The corresponding sampling distributions, color-coded to show the number of minutes in each bin, t_b(m), are shown in the small panels.

analysis showed that ECH waves are excluded from high-density regions inside the plasmpause as can be seen in Figure 2. ECH waves cover a wide range of amplitudes, peaking at the magnetic equator during active conditions but also remaining weakly enhanced outside of the plasmapause during quiet times and at high latitudes. We have therefore used the absence of ECH waves as a criterion to identify high density regions and as a method of distinguishing hiss from chorus waves.

[18] To determine a threshold criterion for ECH waves, we initially inspected the data for orbits 63 to 163 shown in Plate 2 of *Meredith et al.* [2001]. On this plot, the empirical position of the plasmapause, as defined by *Carpenter and Anderson* [1992], is marked as a solid white line. To a first approximation, the empirical plasmapause position separates the enhanced ECH wave amplitudes outside the plasmapause from the background levels seen inside the plasmapause. The background amplitude levels seen inside the plasmapause are typically less than 0.0005 mV m^{-1} which suggests that this would be a good threshold value. During quiet conditions, when the *AE* index has been less than 100 nT for more than 10 hours, the plasmapause position tends to lie well outside $L = 3$. We analyzed the complete ECH wave amplitude database and found that during such conditions, the ECH wave amplitude in the region $2 < L < 3$ is less than 0.0005 mV m^{-1} for ~86% of the time. We therefore use the criterion that the ECH wave amplitude for frequencies in the range $f_{ce} < f < 2f_{ce}$ must be less than 0.0005 mV m^{-1} in order for wave emissions below f_{ce} in the frequency band $0.1 < f < 2$ kHz to be identified as plasmaspheric hiss.

3.2. Variation of Plasmaspheric Hiss Amplitudes During Substorm Activity

[19] Using the database results, we divide the plasmaspheric hiss emissions into two categories: equatorial hiss, defined as emissions between $-15° < \lambda_m < 15°$, and midlatitude hiss, defined as emissions for $15° < |\lambda_m| < 30°$.

3.2.1. MLT Distribution of Equatorial Hiss

[20] The variation of the equatorial hiss amplitudes with substorm activity is shown as a function of L and MLT in Figure 3, at a resolution of $0.1L$ and 1 hour in local time. Average wave amplitudes are plotted in the large panels, and the corresponding sampling distributions are given in the smaller panels. Here, and in the subsequent plots, the sampling distributions represent the time in minutes that CRRES spent in a given bin subject to the given selection criteria. It takes 32.768 s to determine the hiss amplitude, so the number of samples in a given bin may be obtained by multiplying the time in bin by 1.83. The top panels show the average equatorial hiss amplitudes as a function of the instantaneous value of the *AE* index subdivided into the three activity levels $AE < 100$ nT, $100 < AE < 500$ nT and $AE > 500$ nT. The equatorial hiss amplitudes exhibit a

pronounced increase with *AE* and also show a substantial day-night asymmetry. It is also interesting to note how the high-density region determined from the ECH criterion contracts for high levels of *AE*, consistent with the expected location of the plasmapause.

[21] Electrons in the energy range 10–100 keV are expected to play the most significant role in the cyclotron resonant generation of plasmaspheric hiss [e.g., *Church and Thorne*, 1983]. Equatorially mirroring electrons at $L = 3$ with energies in this range take between ~1.5 and ~12 hours to gradient-drift from the region of initial injection in the midnight sector through to the noon sector. If the injected plasmasheet electrons provide the source of free energy for the strongest dayside hiss emissions, there should be a time delay between the onset of substorm activity and the increase in observed wave amplitudes. Similarly, there should be a time delay between the end of substorm activity and the decrease in observed wave amplitudes. For example, if the AE index has just fallen from active values to below 100 nT, then it is likely that recently injected electrons will still be contributing to hiss generation. If, however, the AE index has been below 100 nT for several hours or more, most of the electrons responsible for hiss generation will have had time to drift around dawn to the dayside. We tested this concept by analyzing the observed wave amplitudes with respect to the maximum value of the *AE* index over the time interval Δt prior to the wave observations. By varying Δt we noted that some of the higher wave amplitudes observed for $AE < 100$ nT and for $100 < AE < 500$ nT do not contribute to the distributions when $\Delta t \geq 3$ hours. More quantitatively, this is demonstrated by examining the average equatorial hiss amplitude for $AE < 100$ nT in the region $2 < L < 4.5$, which falls from 19 ± 0.5 pT for $\Delta t = 0$ to 15 ± 0.5 pT for $\Delta t =$ 3 hours. Here, and henceforth, the quoted errors are the standard error of the mean. For larger values of Δt the average value remains around 15 pT in this region. The bottom panels of Figure 3 show the equatorial hiss amplitudes with respect to the maximum value of the *AE* index in the previous 3 hours (*AE**) and confirm that the equatorial hiss amplitudes for $AE^* < 100$ nT and for $100 < AE^* < 500$ nT are generally smaller than those for $AE < 100$ nT and for $100 < AE < 500$ nT. This is due to the finite drift time of the electrons and suggests that electrons above 30 keV are likely to be most important for the generation of hiss.

[22] We will subsequently discuss the properties of hiss using *AE** as the indicator of substorm activity. During quiet conditions ($AE^* < 100$ nT) the average equatorial hiss amplitude in the region $2 < L < 4$ is 17 ± 1 pT, falling to 7 ± 1 pT further out ($4 < L < 6$). Elevated wave amplitudes are seen during moderate conditions ($100 < AE^* < 500$ nT) with an average value of 26 ± 1 pT in the region $2 < L < 4$ between 0600 and 2100 MLT. The equatorial hiss is most enhanced and covers the largest region of geospace during active conditions ($AE^* > 500$ nT) with an average amplitude of 40 ± 1 pT in the region $2 < L < 4$ from 0600 to 2100 MLT. During these conditions the peak values can exceed 100 pT. These results clearly show that the equatorial hiss emissions are substorm-dependent.

3.2.2. MLT Distribution of Midlatitude Hiss

[23] Midlatitude hiss is shown as a function of *L*, MLT, and substorm activity in Figure 4. As before, the top and bottom panels show the average midlatitude hiss amplitudes as a function of *AE* and *AE**, respectively. Some of the higher wave amplitudes observed for $AE < 100$ nT and for $100 < AE < 500$ nT do not contribute to the distributions for $AE^* < 100$ nT and for $100 < AE^* < 500$ nT. Thus the midlatitude hiss is also better ordered using *AE** as opposed to the instantaneous value of the *AE* index.

[24] During quiet conditions the average midlatitude hiss amplitude in the region $2 < L < 4$ is 24 ± 1 pT. At larger *L*, the amplitudes can fall below 1 pT around dusk but remain of the order of 10 pT around dawn. Elevated amplitudes are seen during moderate conditions particularly in the range $2 < L < 4$ between 0600 and 1400 MLT where the average amplitude is 43 ± 2 pT. There is also evidence for a distinct region of enhanced midlatitude hiss at $L > 5$ in the afternoon sector between 1200 and 1800 MLT, which is not seen in the equatorial distribution (Figure 3). However, the midlatitude hiss is most enhanced and covers the largest region of geospace during active conditions, with an average amplitude of 47 ± 2 pT in the region $2 < L < 4$ from 0800 to 1800 MLT. Strong emissions extend out beyond $L = 6$ from 1200 to 1500 MLT, with an average amplitude of 81 ± 6 pT in the region $4 < L < 6$ from 1200 to 1500 MLT. During active conditions the peak values can again exceed 100 pT. These results confirm that the midlatitude hiss emissions are also substorm-dependent. The enhanced emissions extending to high *L* are not observed in the distribution of equatorial hiss in Figure 3. Inspection of the appropriate spectrograms reveals that these waves are hiss and not whistler mode chorus. They may be associated with regions related to enhanced density plumes or detached plasma.

3.3. Latitudinal Distribution of Hiss

[25] Comparison of equatorial and midlatitude hiss distributions suggest there is an important latitudinal dependence. To study the latitudinal dependence in more detail, we have divided the MLT coverage into two sectors, 0600 to 2100 MLT, corresponding to high wave amplitudes, and 2100 to 0600 MLT, corresponding to lower wave amplitudes.

3.3.1. Dawn to Evening Sector 0600–2100 MLT

[26] The average plasmaspheric hiss amplitudes from the dawn to evening sector (0600–2100 MLT) are shown as a function of the radial distance from the center of the Earth projected onto the plane of the magnetic equator, x, GSM z, and substorm activity in the upper panels of Figure 5. Dipole field lines and lines of constant magnetic latitude are included on the plot to help visualize the behavior of the wave amplitudes as a function of *L* and magnetic latitude. As before, the average amplitudes are plotted in the large panels and the corresponding sampling distributions in the small panels. There are two regions of enhanced hiss emissions, one in the equatorial region, and the other at higher latitudes for $20° < |\lambda_m| < 30°$.

[27] The equatorial hiss peaks within about ±5° of the magnetic equator in the range $2 < L < 5$. The amplitudes in this region increase with *AE** (middle and right panels) and tend to broaden in latitude with an increase in *AE**. During quiet and moderate conditions the average amplitudes are 17 ± 1 pT and 28 ± 1 pT, respectively. The equatorial hiss is most enhanced during active conditions in the region $2 < L <$ 4.5 for $|\lambda_m| < 5°$ with an average amplitude of 53 ± 2 pT. The peak equatorial emissions are narrower in latitude than our

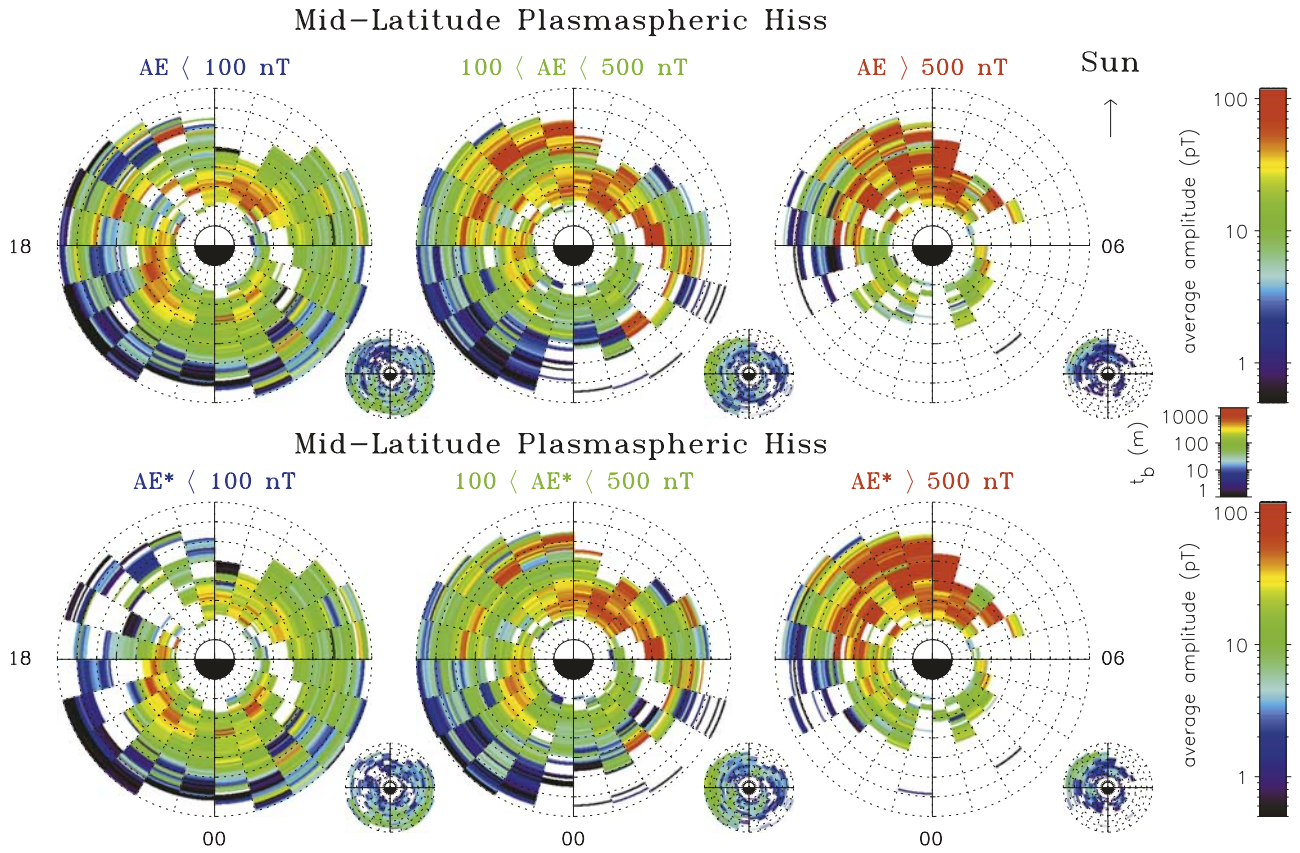

Figure 4. The average midlatitude hiss magnetic field wave amplitude as a function of L, MLT, and substorm activity in the same format as Figure 3.

definition of equatorial hiss used above and therefore must dominate the MLT distributions shown in Figure 3.

[28] The midlatitude hiss peaks in the latitude range $20° < |\lambda_m| < 30°$ in the region $2 < L < 6$. Here the largest emissions are confined to the region $2 < L < 4$ during quiet and moderate conditions but extend out beyond $L = 6$ during active conditions. For example, the average wave amplitudes in the region $2 < L < 4$ increase from 30 ± 1 pT to 44 ± 1 pT and 46 ± 2 pT during quiet, moderate, and active conditions, respectively. Further out, in the region $4 < L < 6$ the average hiss amplitudes are less than 20 pT during quiet and moderate conditions but rise to 65 ± 5 pT during active conditions.

[29] For low and moderate activity, hiss is generally confined within the region $2 < L < 5$ with a distinct minimum in hiss amplitudes in the latitude range $5° < |\lambda_m| < 20°$. For moderate conditions, there is a region $2 < L < 4$ where hiss amplitudes peak for latitudes $20° < |\lambda_m| < 30°$, whereas for $4 < L < 5$ hiss is strongest at the equator. Conversely, for active conditions, for $L > 4.5$, hiss emissions peak in the latitude range $15° < |\lambda_m| < 30°$ again and have a minimum near the equator. This suggests that the two regions of enhanced emissions may have a different origin.

3.3.2. Nightside Sector 2100–0600 MLT

[30] The average plasmaspheric hiss amplitudes in the nightside sector (2100–0600 MLT) are shown in a similar format in the lower panels of Figure 5. The average amplitudes are of the order of 15 pT in the region $2 < L < 5$ with evidence for localized regions of enhanced amplitudes both near the equator and at higher latitudes. The equatorial emissions increase with substorm activity whereas the midlatitude emissions appear to peak during quiet conditions. However, the regions of enhanced hiss are not as strong or as extensive as those observed in the dawn to evening sector. At larger L ($5 < L < 7$) the average amplitudes are of the order of 5 pT during quiet and moderate conditions. There is only sparse data coverage in this region during active conditions.

4. Electron Minimum Resonant Energies

[31] The pronounced enhancement of plasmaspheric hiss amplitudes with increasing substorm activity suggests an excitation mechanism associated with enhanced convective injection of plasma sheet electrons during substorm activity, followed by gradient/curvature drift to the dayside. The source of free energy for wave excitation can be provided by natural gradients in the electron distribution function in the vicinity of the loss cone or by thermal anisotropy produced by the inward transport. Cyclotron resonant amplification will be enhanced as additional resonant electrons are injected into the inner magnetosphere following substorm activity.

[32] To identify the source population for hiss, we follow the method described by *Meredith et al.* [2003b] (section 3) and evaluate the electron minimum resonant energies for first-order cyclotron resonance with parallel-propagating R-mode waves in an electron-proton plasma. We use f_{pe} derived from the wave instrument and f_{ce} from the

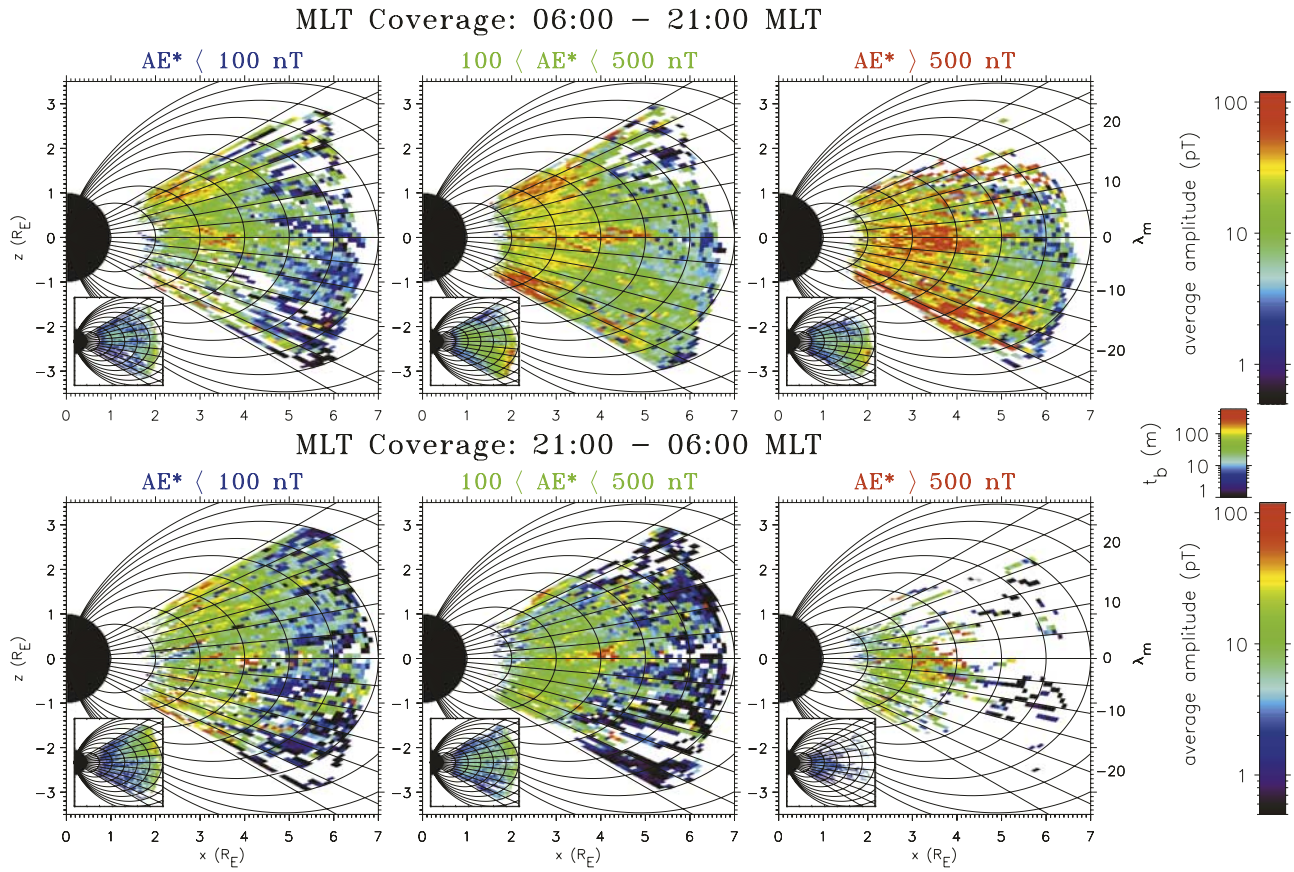

Figure 5. The average radial and latitudinal distribution of plasmaspheric hiss magnetic field wave amplitude as a function of *AE** for 0600–2100 MLT (upper panels) and 2100–0600 MLT (lower panels).

magnetometer. The results for the equatorial region are shown as a function of L, MLT, and *AE** in the top panels of Figure 6 for a wave frequency of 600 Hz. For a typical band of hiss between 200 Hz and 2 kHz, the range of minimum resonant energies lie within a factor of ~3 above or below the values shown. In the equatorial region cyclotron minimum resonant energies vary from about 20 keV near $L = 6$ to about 1 MeV near $L = 2$. In the midlatitude region, cyclotron minimum resonant energies (not shown) typically vary from about 50 keV near $L = 6$ to 2 MeV near $L = 2$. Since the flux of ~MeV electrons is generally too low to cause significant wave amplification, the waves observed for $L < 3$ must propagate into the inner magnetosphere from a source region located further out [e.g., *Thorne et al.*, 1979]. However, the presence of hiss at low L can still cause pitch-angle scattering and loss of relativistic (~MeV) electrons in the slot region [*Lyons et al.*, 1972; *Abel and Thorne*, 1998a, 1998b].

[33] The ratio f_{pe}/f_{ce} is a critical parameter that not only determines the range of resonant energies for a given band of hiss (see Figure 1) but also determines whether whistler mode waves contribute efficiently to electron loss or acceleration [*Summers et al.*, 1998]. Low values of this ratio ($f_{pe}/f_{ce} < \sim 3$) are required for efficient acceleration [e.g., *Summers et al.*, 1998; *Horne et al.*, 2003b]. The equatorial ratio f_{pe}/f_{ce}, subject to the criterion $E_{ECH} < 0.0005$ mV m^{-1}, is shown in the lower panels of Figure 6. The ratio f_{pe}/f_{ce} is primarily greater than 5 in the region $L > 2.5$ but decreases to ~3.5 at $L = 2$. This indicates that hiss may contribute to electron precipitation into the atmosphere but does not provide efficient electron acceleration.

4.1. Global Distribution of Energetic Electrons

[34] The average equatorial electron perpendicular differential number flux, $J_\perp$, is shown as a function of L, MLT, and *AE** for three different energies in Figure 7 to determine whether the increase in hiss amplitudes is also associated with an increase in the resonant electron flux. The flux at 1.09 keV (lower panels) is representative of the electrons responsible for the Landau damping of hiss while the flux at 28.5 keV (middle panels) and 153 keV (upper panels) is representative of the electons responsible for the cyclotron resonant generation of hiss. To illustrate the changes in electron flux with *AE** throughout the inner magnetosphere, we do not apply the ECH criterion but rather use all of the data in Figure 7. The substorm convection electric fields dominate the motion of the 1.09 keV electrons, whereas convection electric fields, gradient, and curvature drifts all contribute to the motion of 28.5 keV and 153 keV electrons [e.g., *Roederer*, 1970].

[35] The three bottom panels of Figure 7 show that the flux of 1.09 keV electrons is most enhanced during substorm activity in the region $4 < L < 6$ between 2100 and 0700 MLT. The flux of injected low-energy electrons is substantially reduced at 1200 MLT, and there is virtually no enhancement in the afternoon sector. Conversely, for $L < 4$ there is little or no substorm dependence for the flux at

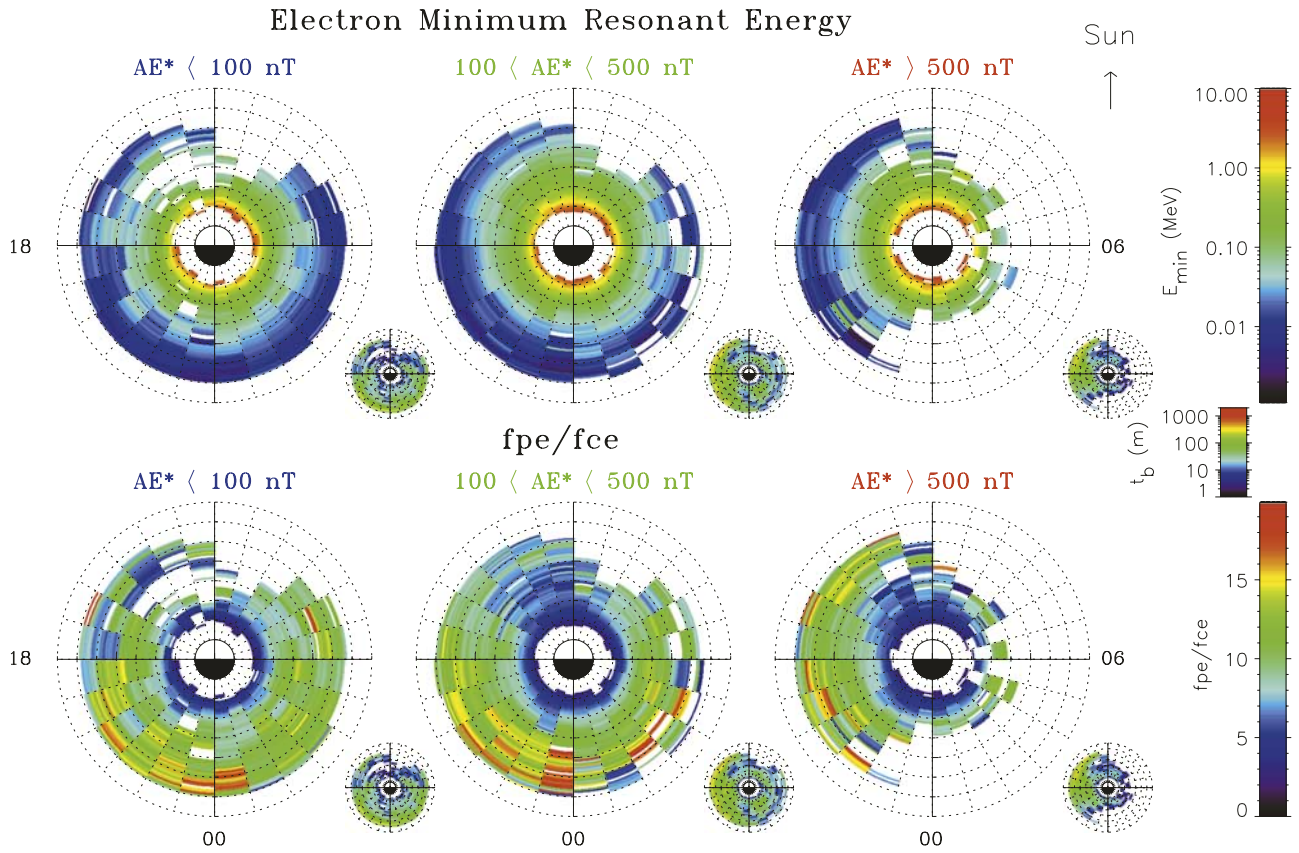

Figure 6. The equatorial electron minimum resonant energies for plasmaspheric hiss at 600 Hz (upper panels) and the equatorial ratio f_{pe}/f_{ce} (lower panels) as a function of L, MLT, and AE*.

1.09 keV. This is to be expected since ~1 keV electrons do not easily penetrate inside the plasmapause. The flux typically lies in the range 10^6–10^7 cm^{-2} s^{-1} sr^{-1} keV^{-1} over the entire inner magnetosphere. Thus since ~1 keV electrons inside the plasmapause are not enhanced, they cannot play a significant role in the generation of plasmaspheric hiss, but they could contribute to Landau damping [e.g., *Church and Thorne*, 1983; *Thorne and Horne*, 1994].

[36] At 28.5 keV the flux increases with AE* (Figure 7, middle panels), particularly for $L > 4$ between 2200 and 0800 MLT for active conditions. Again, the flux increase is substantially reduced as MLT increases, but these higher-energy electrons penetrate further around into the afternoon sector. At 153 keV (Figure 7, upper panels) there is a clear substorm-dependent flux enhancement, mainly outside $L = 3$, for all MLT. These higher energy electrons can penetrate to lower L by enhanced radial diffusion [e.g., *Liu et al.*, 2003]. For active conditions there in an enhancement near dawn, for $4 < L < 6$, which is due to a very large event during the early orbits of CRRES.

[37] Summary plots of the hiss amplitudes, the minimum resonant energies for hiss at 600 Hz, and the electron flux ratios at 28.5 keV and 153 keV for the equatorial region during active conditions are shown in Figure 8. The electron flux ratio, defined to be the flux ratio between active (AE* > 500 nT) and quiet (AE* < 100 nT) conditions, represents the flux change between active and quiet times. We have also applied the criterion $E_{ECH} < 0.0005$ mV m^{-1} to the analysis of the particle data to study the relationship between the enhanced hiss and the increase in the particle flux inside the plasmapause. Thus the energetic electron flux ratios are only shown for the high-density regions where we have identified the hiss.

[38] Since the minimum resonant energies for a typical band of hiss between 200 Hz and 2 kHz lie within a factor of ~3 above or below the plotted values, we infer that the minimum resonant energies fall below 30 keV outside $L \sim 5$. Here, in the afternoon sector where data is available and the equatorial hiss is weakly enhanced, the average flux ratio of 28.5 keV electrons is 1.5 ± 0.1. The enhancement of these electrons is relatively small but may contribute to the generation of the weakly enhanced hiss observed in this region. The minimum resonant energies for the same band of hiss fall below ~153 keV outside $L \sim 3$. Enhanced fluxes of 153 keV electrons are commonly observed in this region. For example, the flux of these electrons increases by a factor of 3 ± 0.1 in the region $3.5 < L < 4.5$ between 1600 and 2100 MLT. The equatorial hiss is also enhanced in this region, suggesting that the enhancements in the ~150 keV electron flux may play an important role in the generation of hiss. In the midlatitude region (not shown) there is also evidence for enhanced fluxes of 28.5 keV and 153 keV electrons associated with the enhanced fluxes of midlatitude hiss.

5. Discussion

[39] Previous theoretical studies [*Church and Thorne*, 1983; *Huang et al.*, 1983] suggested that plasmaspheric

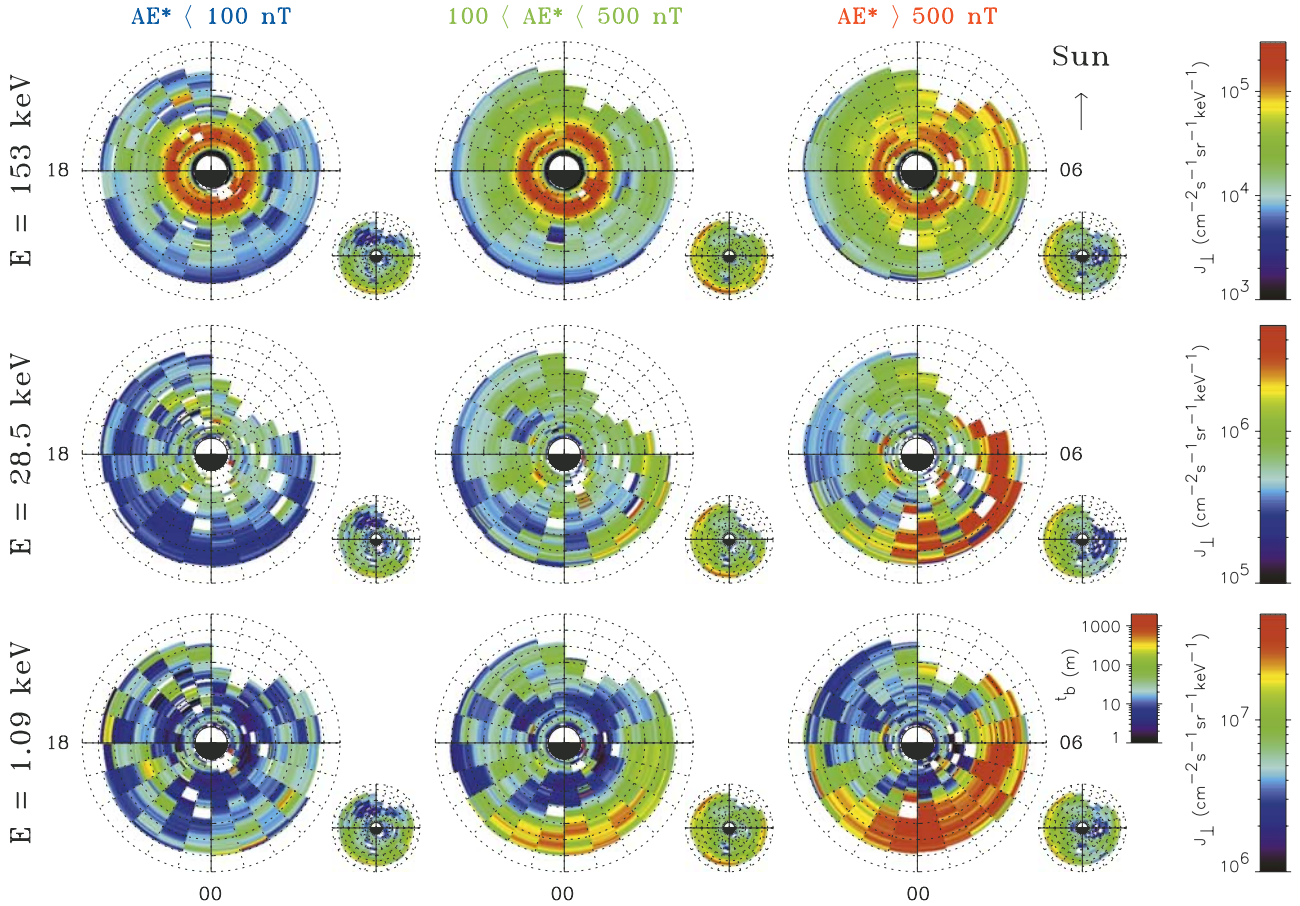

Figure 7. The average electron perpendicular number flux as a function of L, and MLT and AE^* for 1.09 keV (bottom panels), 28.5 keV (middle panels), and 153 keV (top panels) electrons.

hiss is generated by cyclotron resonant instability with 10–100 keV electrons in a localized region just inside the plasmapause. The waves subsequently propagate inwards to lower L, filling most of the plasmasphere. The source population was assumed to be injected from the plasma sheet during substorm activity. Such electrons are preferentially injected at midnight and then drift around to the dayside where they encounter the plasmapause and generate hiss. This result is tentatively supported by the distribution of enhanced plasmaspheric hiss during active times (Figure 7), which shows an MLT dependence that could be attributed to this mechanism. However, the mechanism for the generation of hiss is more complicated than originally thought. Our analysis of the global distribution of low-energy resonant electrons observed on CRRES indicates that electrons below ~30 keV cannot be the source of the strongest dayside hiss emissions. During active conditions, such electrons appear to be largely removed from the radiation belts before they can drift to the dayside (Figure 8, bottom left). Higher energy electrons exhibit much less MLT dependence, and the flux of 153 keV electrons observed on CRRES is significantly enhanced in the region where strong dayside hiss is observed (Figure 8, bottom right), indicating that such electrons contribute to the source population for dayside hiss. This is also consistent with our estimates of cyclotron resonant energies based on measured electron densities just inside the plasmapause (Figure 8, top right). Higher-energy electrons will also play a role in the generation of hiss but will become increasingly less important as the absolute flux decreases. Our results suggest that the key electron energy range for the generation of hiss is tens to hundreds of keV. We are unable to asses the role of electrons in the energy range from 30 to 153 keV in the generation of hiss due to the lack of reliable electron measurements in this energy range inside $L \sim 6$.

[40] Plasmaspheric hiss has a pronounced local time dependence. In the dawn to evening sector (0600–2100 MLT), hiss is far more intense and is associated with enhanced fluxes of electrons with energies in the range of tens to hundreds of keV. In the nighttime sector (2100–0600 MLT) the hiss is much weaker and confined to lower L for increasing substorm activity (Figure 5). After an active period the convection electric field diminishes and hiss may be excited on the nightside as the plasmapause moves out to larger L, overlapping with the enhanced flux of energetic electrons.

[41] Previous ray-tracing studies indicate that whistler-mode waves should become highly oblique as they propagate from an equatorial source region to higher latitude. Landau damping by resonant (<1 keV) electrons should consequently become important [e.g., *Church and Thorne*, 1983] away from the equator. CRRES observations indicate a large increase in the flux of Landau resonant electrons on the nightside for $L > 3$ during substorm conditions

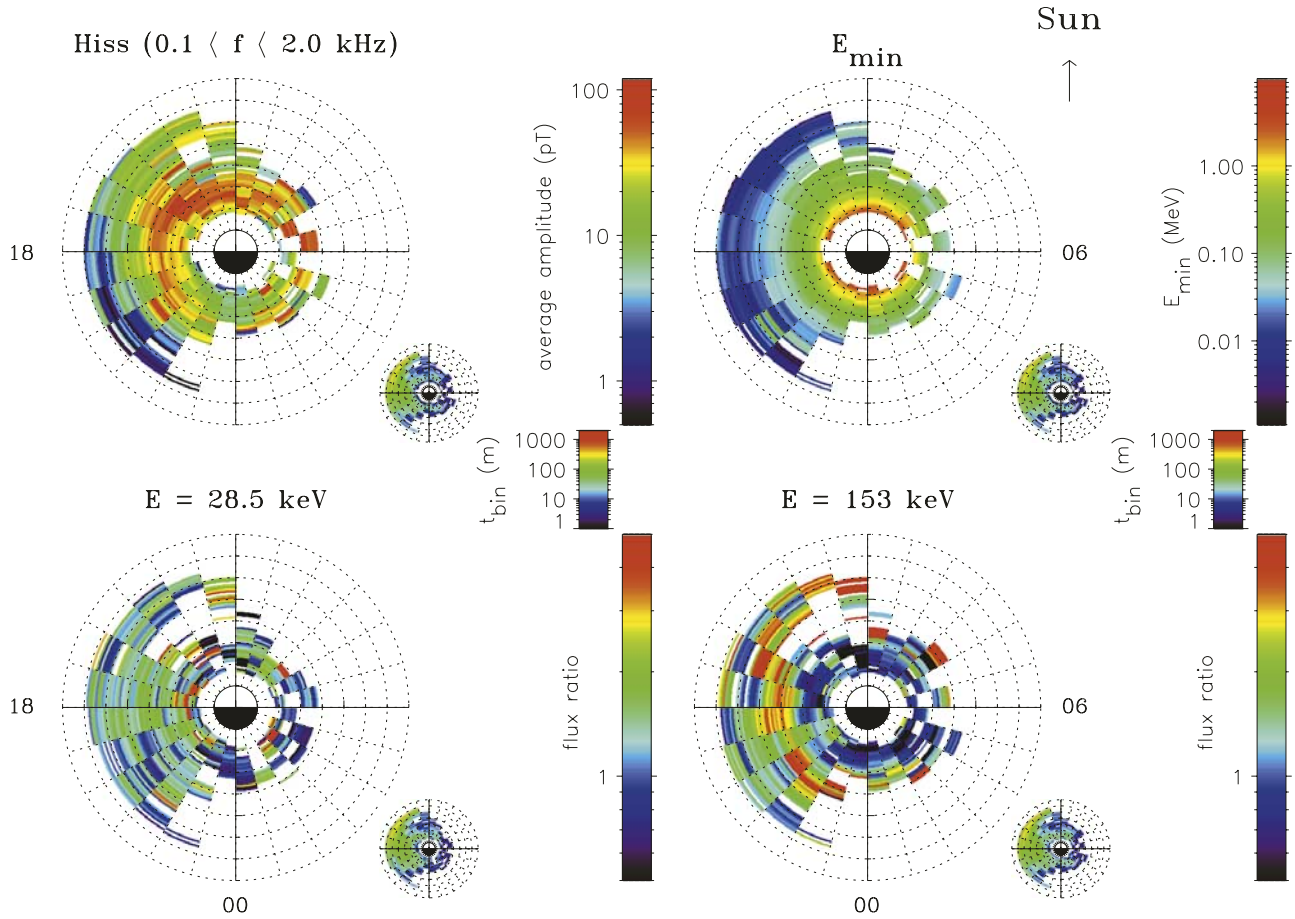

Figure 8. Summary plot of the equatorial distribution of hiss (top left), minimum resonant electron energies (top right), and the ratio of the flux during active conditions ($AE^* > 500$ nT) to the flux during quiet conditions ($AE^* < 100$ nT) for 28.5 keV electrons (bottom left) and 153 keV electrons (bottom right) as a function of L, MLT. The hiss amplitudes and the electron minimum resonant energies are shown for active conditions.

(Figure 7), and the presence of these low-energy electrons will confine any nightside hiss to the equatorial region as observed. This concept also raises the interesting question of whether the pronounced day/night difference in the latitudinal distribution of hiss could in part be due to the absence of any significant substorm related injection of low-energy Landau resonant electrons on the dayside, since waves could then become highly oblique without experiencing significant damping.

[42] An alternative suggestion for the origin of plasmaspheric hiss involves the magnetospheric reflection of whistlers originating from lightning [*Draganov et al.*, 1992]. The idea is that if the lightning rate is sufficiently high and if whistlers remain undamped for a sufficiently long period, then after many magnetospheric reflections whistlers would merge into a continuum which would look like hiss when observed on a spacecraft. Ray-tracing shows that such magnetospherically reflected (MR) whistlers become obliquely propagating and that if the flux of ~1 keV electrons is included, then the lifetime of MR whistlers is significantly reduced through electron Landau damping [*Thorne and Horne*, 1994]. Others have argued that inside the plasmasphere the flux of 1 keV electrons is not prohibitive [*Bell et al.*, 2002]. However, the most striking feature of the data presented here is the strong dependence of hiss amplitudes on the level of substorm activity. A lightning source is independent of substorm activity. Although lightning rates may be higher in the afternoon due to local thunderstorm activity, wave absorption in the ionosphere is approximately 10 dB higher on the dayside compared with that on the nightside [*Smith and Jenkins*, 1998]. At best, a lightning source could only account for the quiet-time levels of hiss. Thus the strong dependence of hiss on substorm activity would seem to rule out a lightning source and favor generation by cyclotron resonant interactions with substorm injected electrons.

[43] The latitudinal distribution of hiss in the dawn to evening sector raises an interesting question concerning the origin of hiss. If hiss is generated near the equatorial region and propagates to higher latitudes [e.g., *Church and Thorne*, 1983; *Parrot and Lefeuvre*, 1986; *Cornilleau-Wehrlin et al.*, 1993; *Santolik et al.*, 2001], then this theory cannot account for the minimum in wave power between equatorial and midlatitude hiss observed for quiet and moderate activity for $L < 4$. The minimum in wave power is still present for $L < 4$ under active conditions but less pronounced. It may be possible that the increase in wave spectral intensity near 25° could be due to a propagation effect associated with the

magnetospheric reflection of the waves as the frequency drops below the lower hybrid. However, midlatitude hiss is much stronger than that in the equatorial region for $L > 5$, under moderate and active conditions, and therefore this suggestion cannot explain both sets of observations. The two distinct latitudinal zones of enhanced hiss emissions in the dawn to evening sector suggest two source regions. One is confined to low latitudes $|\lambda_m| < 5°$, the other is confined to latitudes $20 < |\lambda_m| < 30°$, and both depend on geomagnetic activity. In both cases, the generation mechanism must be related to substorm activity. If hiss is generated in two source regions, then this may also be related to observations where hiss wave normal angles have two populations, one close to field-aligned, and the other at large angles near the Gendrin angle [e.g., *Storey et al.*, 1991; *Santolik et al.*, 2001]. More data on the distribution of wave normal angles, as a function of latitude and substorm activity, are required to investigate this possibility in detail.

[44] There is one unavoidable bias in the statistical data presented in this study. There was a much higher level of geomagnetic activity during the latter part of the CRRES mission. This may account in part for the apparent higher level of hiss in the postnoon sector compared with prenoon. However, the sampling of the day and night time sectors is such that it should not affect our conclusions on the local time dependence or on the latitudinal distribution of the waves. Otherwise our results on the global distribution of hiss are entirely consistent with the distribution of steady low-frequency noise [*Russell et al.*, 1969] and plasmapheric hiss [*Thorne et al.*, 1973] reported from OGO 3 observations.

[45] The processes responsible for the slot region between the inner and outer electron radiation belts involve a delicate balance between source and loss mechanisms [*Lyons and Thorne*, 1973]. Previous studies [*Thorne et al.*, 1979] have demonstrated that in the absence of strong Landau damping, waves excited near the plasmapause can subsequently propagate into the inner magnetosphere and there precipitate much higher resonant energy electrons. Our calculations indicate that the equatorial minimum resonant energies can exceed an MeV inside $L = 3$. Since the minimum resonant energy decreases with increasing L, the data here suggest that the outer boundary of the quiet time slot region should be found at progressively higher L values for decreasing energies, as previously observed [e.g., *Lyons et al.*, 1972; *Horne et al.*, 2003a].

[46] The equatorial minimum resonant energies with a band of plasmaspheric hiss ($0.2 < f < 2$ kHz) typically exceed 1 MeV inside $L = 3$ and fall into the range 100 keV $< E <$ 300 keV in the region $3 < L < 5$. The midlatitude minimum resonant energies typically exceed 1 MeV inside $L = 4$ and fall into the range 100 keV $< E <$ 300 keV in the region $3 < L < 6.5$. Outer zone electrons with energies of the order of a few hundred keV form the "seed" population of electrons [e.g., *Baker et al.*, 1998a, 1998b; *Obara et al.*, 2000] which may be subsequently energized to MeV energies by substorm-enhanced whistler mode chorus waves [e.g., *Horne and Thorne*, 1998, 2003; *Summers et al.*, 1998, 2002, 2004; *Summers and Ma*, 2000; *Horne*, 2002; *Meredith et al.*, 2002a, 2003a, 2003c; *Miyoshi et al.*, 2003; *O'Brien et al.*, 2003]. *Summers et al.* [1998] proposed a model for the gradual acceleration of electrons to relativistic energies during the recovery phase of geomagnetic storms which involved a combination of energy diffusion by enhanced whistler mode chorus outside of the plasmasphere and enhanced pitch-angle scattering by electromagnetic ion cyclotron (EMIC) waves near the duskside plasmapause. Recent theoretical and experimental work has shown that EMIC waves may indeed play an important role in the loss of relativistic electrons during enhanced geomagnetic activity [*Lorentzen et al.*, 2000; *Albert*, 2003; *Meredith et al.*, 2003b; *Summers and Thorne*, 2003]. It is clear from the present study that enhanced levels of plasmaspheric hiss will also contribute to pitch-angle scattering inside the plasmasphere. This paper provides the basis for calculating timescales for pitch-angle scattering of relativistic electrons by plasmaspheric hiss. We reemphasize here that modeling the behavior of relativistic electrons during storms requires detailed accounting of electron losses to the atmosphere by all classes of plasma waves present.

6. Conclusions

[47] We have performed a statistical analysis of plasmaspheric hiss, the ratio f_{pe}/f_{ce}, the associated minimum resonant energies, and the electron fluxes using data from wave and particle instruments on board the CRRES spacecraft. Our main conclusions are as follows:

[48] 1. Plasmaspheric hiss amplitudes are dependent on L shell, MLT, latitude, and substorm activity, with two distinct latitudinal zones of peak wave activity, primarily on the dayside.

[49] 2. Equatorial hiss ($|\lambda_m| < 15°$) is strongest during active conditions with an average amplitude of 40 ± 1 pT in the region $2 < L < 4$ from 0600 to 2100 MLT. Midlatitude ($|\lambda_m| > 15°$) hiss is strongest during active conditions with an average amplitude of 47 ± 2 pT in the region $2 < L < 4$ from 0800 to 1800 MLT but extending out beyond $L = 6$ from 1200 to 1500 MLT. We conclude that hiss must be generated by cyclotron resonant interactions with substorm-injected electrons.

[50] 3. The hiss amplitudes peak in two latitude regions in the dawn to evening sector. Equatorial hiss peaks within $\pm 5°$ of the magnetic equator between $2 < L < 5$. Midlatitude hiss peaks in the latitude range $20° < |\lambda_m| < 30°$, predominantly in the region $2 < L < 4$ between 0800 and 1800 MLT but extending beyond $L = 6$ between 1200 and 1500 MLT. We suggest that plasmaspheric hiss may be generated in two source regions, one near the equator and the other at midlatitudes. Further measurements on the distribution of wave normal angles as a function of latitude and magnetic activity would be required to examine this possibility in detail.

[51] 4. Enhanced equatorial hiss has minimum resonant energies from $\sim$0.1 MeV at $L = 4$ to $\sim$1 MeV at $L = 2$ to within a factor of 3. Enhanced midlatitude hiss has minimum resonant energies from $\sim$0.05 MeV at $L = 6$ to $\sim$2 MeV at $L = 2$ to within a factor of 3.

[52] 5. The enhanced equatorial and midlatitude hiss emissions are associated with electron flux enhancements in the energy range of tens to hundreds of keV and not with $\sim$1 keV electrons. We suggest that the key electron energy range for the generation of hiss is tens to hundreds of keV, since these electrons can penetrate into the high-density regions.

[53] 6. Just inside the plasmapause, where the hiss is observed, the ratio f_{pe}/f_{ce} is large and typically greater than 5. We conclude that plasmaspheric hiss does not contribute to electron acceleration. However, as the minimum resonant energy increases with decreasing L, hiss will contribute to electron loss into the atmosphere at energies up to ~1 MeV at lower L and particularly to the formation of the slot region following geomagnetic storms.

[54] **Acknowledgments.** We thank Al Vampola and Daniel Heynderickx for providing the MEA data and Chris Mouikis for providing the IDL software to analyze the LEPA data. We also thank the World Data Centre C1 for STP at the Rutherford Appleton Laboratory and the NSSDC Omniweb for providing the geomagnetic indices used in this paper. This research was funded in part by the UK Natural Environment Research Council, NSF grant ATM-0101159, NASA grants NAG5-11922 and NAG5-11826. D. S. acknowledges support from the Natural Sciences and Engineering Research Council of Canada under grant A-0621.

[55] Shadia Rifai Habbal thanks Nicole Cornilleau-Wehrlin and another referee for their assistance in evaluating this paper.

References

Abel, B., and R. M. Thorne (1998a), Electron scattering loss in Earth's inner magnetosphere: 1. Dominant physical processes, *J. Geophys. Res.*, *103*, 2385.

Abel, B., and R. M. Thorne (1998b), Electron scattering loss in Earth's inner magnetosphere: 2. Sensitivity to model parameters, *J. Geophys. Res.*, *103*, 2397.

Albert, J. M. (1994), Quasi-linear pitch angle diffusion coefficients: Retaining high harmonics, *J. Geophys. Res.*, *99*, 23,741.

Albert, J. M. (2003), Evaluation of quasi-linear diffusion coefficients for EMIC waves in a multi-species plasma, *J. Geophys. Res.*, *108*(A6), 1249, doi:10.1029/2002JA009792.

Anderson, R. R., D. A. Gurnett, and D. L. Odem (1992), CRRES plasma wave experiment, *J. Spacecr. Rockets*, *29*, 570.

Baker, D. N., et al. (1998a), A strong CME-related magnetic cloud interaction with the Earth's magnetosphere: ISTP observations of a rapid relativistic electron acceleration on May 15, 1997, *Geophys. Res. Lett.*, *25*, 2975.

Baker, D. N., X. Li, J. B. Blake, and S. G. Kanekal (1998b), Strong acceleration in the Earth's magnetosphere, *Adv. Space. Res.*, *21*, 609.

Bell, T. F., U. S. Inan, J. Bortnik, and J. D. Scudder (2002), The Landau damping of magnetospherically reflected whistlers within the plasmasphere, *Geophys. Res. Lett.*, *29*(15), 1733, doi:10.1029/2002GL014752.

Belmont, G., D. Fontaine, and P. Canu (1983), Are electron cyclotron waves responsible for diffuse auroral electron precipitation, *J. Geophys. Res.*, *88*, 9163.

Carpenter, D. L., and R. R. Anderson (1992), An ISEE/whistler model of equatorial electron density in the magnetosphere, *J. Geophys. Res.*, *97*, 1097.

Chan, K. W., and R. E. Holzer (1976), ELF hiss associated with plasma density enhancements in the outer magnetosphere, *J. Geophys. Res.*, *81*, 2267.

Church, S., and R. M. Thorne (1983), On the origin of plasmaspheric hiss: Ray path integrated amplification, *J. Geophys. Res.*, *88*, 7941.

Cornilleau-Wehrlin, N., R. Gendrin, F. Lefeuvre, M. Parrot, R. Grard, D. Jones, A. Bahnsen, E. Ungstrup, and W. Gibbons (1978), VLF electromagnetic waves observed onboard GEOS-1, *Space Sci. Rev.*, *22*, 371.

Cornilleau-Wehrlin, N., J. Solomon, A. Korth, and G. Kremser (1993), Generation mechanism of plasmaspheric ELF/VLF hiss: A statistical study from GEOS 1 data, *J. Geophys. Res.*, *98*, 21,471.

Draganov, A. B., U. S. Inan, V. S. Sonwalker, and T. F. Bell (1992), Magnetospherically-reflected whistlers as a source of plasmaspheric hiss, *Geophys. Res. Lett.*, *19*, 233.

Dunckel, N., and R. A. Helliwell (1969), Whistler-mode emissions on the OGO-1 satellite, *J. Geophys. Res.*, *74*, 6371.

Gough, M. P., P. J. Christiansen, G. Martelli, and E. J. Gershuny (1979), Interaction of electrostatic waves with warm electrons at the geomagnetic equator, *Nature*, *279*, 515.

Hardy, D. A., D. M. Walton, A. D. Johnstone, M. F. Smith, M. P. Gough, A. Huber, J. Pantazis, and R. Burkhardt (1993), Low energy plasma analyser, *IEEE Trans. Nucl. Sci.*, *40*, 246.

Horne, R. B. (2002), The contribution of wave-particle interactions to electron loss and acceleration in the Earth's radiation belts during geomagnetic storms, in *URSI Review of Radio Science 1999–2002*, edited by W. R. Stone, pp. 801–828, John Wiley, Hoboken, N. J.

Horne, R. B., and R. M. Thorne (1998), Potential waves for electron scattering and stochastic acceleration to relativistic energies during magnetic storms, *Geophys. Res. Lett.*, *25*, 3001.

Horne, R. B., and R. M. Thorne (2003), Relativistic electron acceleration and precipitation during resonant interactions with whistler-mode chorus, *Geophys. Res. Lett.*, *30*(10), 1527, doi:10.1029/2003GL016973.

Horne, R. B., N. P. Meredith, R. M. Thorne, D. Heynderickx, R. H. A. Iles, and R. R. Anderson (2003a), Evolution of energetic pitch angle distributions during storm-time electron acceleration to MeV energies, *J. Geophys. Res.*, *108*(A1), 1016, doi:10.1029/2001JA009165.

Horne, R. B., S. A. Glauert, and R. M. Thorne (2003b), Resonant diffusion of radiation belt electrons by whistler mode chorus, *Geophys. Res. Lett.*, *30*(9), 1493, doi:10.1029/2003GL016963.

Huang, C. Y., C. K. Goertz, and R. R. Anderson (1983), A theoretical study of plasmaspheric hiss generation, *J. Geophys. Res.*, *88*, 7927.

Kennel, C. F., and F. Engelmann (1966), Velocity space diffusion from weak plasma turbulence in a magnetic field, *Phys. Fluids*, *9*, 2377.

Kennel, C. F., and H. E. Petschek (1966), Limit on stably trapped particle fluxes, *J. Geophys. Res.*, *71*, 1.

Kennel, C. F., and R. M. Thorne (1967), Unstable growth of unducted whistlers propagating at an angle to the geomagnetic field, *J. Geophys. Res.*, *72*, 871.

Liu, S., M. W. Chen, L. R. Lyons, H. Korth, J. M. Albert, J. L. Roeder, P. C. Anderson, and M. F. Thomsen (2003), Contribution of convective transport to stormtime ring current electron injection, *J. Geophys. Res.*, *108*(A10), 1372, doi:10.1029/2003JA010004.

Lorentzen, K. R., M. P. McCarthy, G. K. Parks, J. E. Foat, R. M. Milan, D. M. Smith, R. P. Lin, and J. P. Treilhou (2000), Precipitation of relativistic electrons by interaction with electromagnetic ion cyclotron waves, *J. Geophys. Res.*, *105*, 5381.

Lyons, L. R., and R. M. Thorne (1973), Equilibrium structure of radiation belt electrons, *J. Geophys. Res.*, *78*, 2142.

Lyons, L. R., R. M. Thorne, and C. F. Kennel (1972), Pitch angle diffusion of radiation belt electrons within the plasmasphere, *J. Geophys. Res.*, *77*, 3455.

Meredith, N. P., R. B. Horne, A. D. Johnstone, and R. R. Anderson (2000), The temporal evolution of electron distributions and associated wave activity following substorm injections in the inner magnetosphere, *J. Geophys. Res.*, *105*, 12,907.

Meredith, N. P., R. B. Horne, and R. R. Anderson (2001), Substorm dependence of chorus amplitudes: Implications for the acceleration of electrons to relativistic energies, *J. Geophys. Res.*, *106*, 13,165.

Meredith, N. P., R. B. Horne, R. H. A. Iles, R. M. Thorne, D. Heynderickx, and R. R. Anderson (2002a), Outer zone relativistic electron acceleration associated with substorm-enhanced whistler mode chorus, *J. Geophys. Res.*, *107*(A7), 1144, doi:10.1029/2001JA900146.

Meredith, N. P., R. B. Horne, D. Summers, R. M. Thorne, R. H. A. Iles, D. Heynderickx, and R. R. Anderson (2002b), Evidence for acceleration of outer zone electrons to relativistic energies by whistler mode chorus, *Ann. Geophys.*, *20*, 967.

Meredith, N. P., M. Cain, R. B. Horne, R. M. Thorne, D. Summers, and R. R. Anderson (2003a), Evidence for chorus-driven electron acceleration to relativistic energies from a survey of geomagnetically-disturbed periods, *J. Geophys. Res.*, *108*(A6), 1248, doi:10.1029/2002JA009764.

Meredith, N. P., R. M. Thorne, R. B. Horne, D. Summers, B. J. Fraser, and R. R. Anderson (2003b), Statistical analysis of relativistic electron energies for cyclotron resonance with EMIC waves observed on CRRES, *J. Geophys. Res.*, *108*(A6), 1250, doi:10.1029/2002JA009700.

Meredith, N. P., R. B. Horne, R. M. Thorne, and R. R. Anderson (2003c), Favored regions for chorus-driven electron acceleration to relativistic energies in the Earth's outer radiation belt, *Geophys. Res. Lett.*, *30*(16), 1871, doi:10.1029/2003GL017698.

Miyoshi, Y., A. Morioka, T. Obara, H. Misawa, T. Nagai, and Y. Kasahara (2003), Rebuilding process of the outer radiation belt during the 3 November 1993 magnetic storm: NOAA and EXOS-D observations, *J. Geophys. Res.*, *108*(A1), 1004, doi:10.1029/2001JA007542.

Obara, T., T. Nagatsuma, M. Den, Y. Miyoshi, and A. Morioka (2000), Main phase creation of "seed" electrons in the outer radiation belt, *Earth Planets Space*, *52*, 41.

O'Brien, T. P., K. R. Lorentzen, I. R. Mann, N. P. Meredith, J. B. Blake, J. F. Fennel, M. D. Looper, D. K. Milling, and R. R. Anderson (2003), Energization of relativistic electrons in the presence of ULF power and MeV microbursts: Evidence for dual ULF and VLF acceleration, *J. Geophys. Res.*, *108*(A8), 1329, doi:10.1029/2002JA009784.

Parrot, M., and F. Lefeuvre (1986), Statistical study of the propagation characteristics of ELF hiss observed on GEOS 1, inside and outside the plasmasphere, *Ann. Geophys.*, *4*, 363.

Roederer, J. G. (1970), *Dynamics of Geomagnetically Trapped Radiation*, Springer-Verlag, New York.

Russell, C. T., R. E. Holzer, and E. J. Smith (1969), OGO 3 observations of ELF noise in the magnetosphere: 1. Spatial extent and frequency of occurrence, *J. Geophys. Res.*, *74*, 755.

Santolik, O., M. Parrot, L. R. O. Storey, J. S. Pickett, and D. A. Gurnett (2001), Propagation analysis of plasmaspheric hiss using Polar PWI measurements, *Geophys. Res. Lett.*, *28*, 1127.

Singer, H. J., W. P. Sullivan, P. Anderson, F. Mozer, P. Harvey, J. Wygant, and W. McNeil (1992), Fluxgate magnetometer instrument on the CRRES, *J. Spacecr. Rockets*, *29*, 599.

Smith, A. J., and P. J. Jenkins (1998), A survey of natural electromagnetic noise in the frequency range f = 1–10 kHz at Halley station, Antarctica: 1. Radio atmospherics from lightning, *J. Atmos. Solar Terr. Phys.*, *60*, 263.

Smith, E. J., A. M. Frandsen, B. T. Tsurutani, R. M. Thorne, and K. W. Chan (1974), Plasmaspheric hiss intensity variations during magnetic storms, *J. Geophys. Res.*, *79*, 2507.

Solomon, J., N. Cornilleau-Wehrlin, A. Korth, and G. Kremser (1988), An experimental study of ELF/VLF hiss generation in the Earth's magnetosphere, *J. Geophys. Res.*, *93*, 1839.

Spjeldvik, W. N., and R. M. Thorne (1975), The cause of storm after effects in the middle latitude D region, *J. Atmos. Terr. Phys.*, *37*, 777.

Storey, L. R. O., F. Lefeuvre, M. Parrot, L. Cairo, and R. R. Anderson (1991), Initial survey of the wave distribution functions for plasmaspheric hiss observed by ISEE 1, *J. Geophys. Res.*, *96*, 19,469.

Summers, D., and C. Ma (2000), A model for generating relativistic electrons in the Earth's inner magnetosphere based on gyroresonant wave-particle interactions, *J. Geophys. Res.*, *105*, 2625.

Summers, D., and R. M. Thorne (2003), Relativistic electron pitch-angle scattering by electromagnetic ion cyclotron waves during geomagnetic storms, *J. Geophys. Res.*, *108*(A4), 1143, doi:10.1029/2002JA009489.

Summers, D., R. M. Thorne, and F. Xiao (1998), Relativistic theory of wave-particle resonant diffusion with application to electron acceleration in the magnetosphere, *J. Geophys. Res.*, *103*, 20,487.

Summers, D., C. Ma, N. P. Meredith, R. B. Horne, R. M. Thorne, D. Heynderickx, and R. R. Anderson (2002), Model of the energization of outer-zone electrons by whistler mode chorus during the October 9, 1990 geomagnetic storm, *Geophys. Res. Lett.*, *29*(24), 2174, doi:10.1029/2002GL016039.

Summers, D., C. Ma, N. P. Meredith, R. B. Horne, R. M. Thorne, and R. R. Anderson (2004), Modeling outer-zone relativistic electron response to whistler-mode chorus activity during substorms, *J. Atmos. Solar Terr. Phys.*, *66*, 133.

Thorne, R. M., and J. N. Barfield (1976), Further observational evidence regarding the origin of plasmaspheric hiss, *Geophys. Res. Lett.*, *3*, 29.

Thorne, R. M., and R. B. Horne (1994), Landau damping of magnetospherically reflected whistlers, *J. Geophys. Res.*, *99*, 17,249.

Thorne, R. M., and C. F. Kennel (1967), Quasi-trapped VLF propagation in the outer magnetosphere, *J. Geophys. Res.*, *72*, 857.

Thorne, R. M., E. J. Smith, R. K. Burton, and R. E. Holzer (1973), Plasmaspheric hiss, *J. Geophys. Res.*, *78*, 1581.

Thorne, R. M., E. J. Smith, K. J. Fiske, and S. R. Church (1974), Intensity variation of ELF hiss and chorus driving isolated substorms, *Geophys. Res. Lett.*, *1*, 193.

Thorne, R. M., S. R. Church, W. J. Malloy, and B. T. Tsurutani (1977), The local time variation of ELF emissions during periods of substorm activity, *J. Geophys. Res.*, *82*, 1585.

Thorne, R. M., S. R. Church, and D. J. Gorney (1979), On the origin of plasmaspheric hiss: The importance of wave propagation and the plasmapause, *J. Geophys. Res.*, *84*, 5241.

Tsurutani, B. T., and E. J. Smith (1974), Postmidnight chorus: A substorm phenomenon, *J. Geophys. Res.*, *79*, 118.

Vampola, A. L., J. V. Osborn, and B. M. Johnson (1992), CRRES magnetic electron spectrometer, *J. Spacecr. Rockets*, *29*, 592.

R. R. Anderson, Department of Physics and Astronomy, University of Iowa, Iowa City, Iowa, IA 52242-1479, USA. (roger-r-anderson@uiowa.edu)

R. B. Horne, British Antarctic Survey, Natural Environment Research Council, Madingley Road, Cambridge, CB3 0ET, UK. (r.horne@bas.ac.uk)

N. P. Meredith, Mullard Space Science Laboratory, University College London, Holmbury St. Mary, Dorking, Surrey, RH5 6NT, UK. (npm@mssl.ucl.ac.uk)

D. Summers, Department of Mathematics and Statistics, Memorial University of Newfoundland, St. John's, Newfoundland, A1C 5S7, Canada. (dsummers@math.mun.ca)

R. M. Thorne, Department of Atmospheric Sciences, University of California, Los Angeles, 405 Hilgard Avenue, Los Angeles, CA 90095-1565, USA. (rmt@atmos.ucla.edu)